Design optimization of energy hubs for third and fourth generation district heating: Uncertainty analysis by dynamic simulation

Moritz Zuschlag, Rawad Hamze, Philipp Althaus and Dirk Müller

Institute for Energy Efficient Buildings and Indoor Climate, E.ON Energy Research Center, RWTH Aachen University, Aachen, Germany, moritz.zuschlag@eonerc.rwth-aachen.de, CA

Abstract:

The expansion of district heating is expected to contribute to reducing CO_2 emissions in the future. District heating networks operating in island mode rely on local heat generation within energy hubs. Linear optimization models are well suited for sizing energy hub components. In design optimization problems, system operation is typically represented using typical days derived from clustered time-series data, together with assumed component efficiencies. An alternative representation of system operation is provided by dynamic simulations, which enable a more detailed modelling of an energy hub and its operation. However, this approach also requires the implementation of appropriate control strategies in addition to the heat generation models. This paper investigates the extent to which the two methods differ in their representation of operation by presenting a techno-economic analysis. The energy hub configurations are optimally designed with the objective of minimizing the net present value, using hourly time-series data describing domestic hot water and space heating demands. Different retrofit states are associated with specific district heating network temperatures. The primary heat supplier is a centralized air-source heat pump, supported by different secondary heat suppliers. Constraints on the heat supply mix are derived from legal regulations. Dynamic simulations use optimization results for system parameterization. The results obtained with both linear optimization and dynamic simulation are analyzed and compared. The techno-economic analysis evaluates differences in decision-relevant indicators arising from the operational representations, based on annual energy demand, peak electric power, and the levelized cost of heat. Differences up to 3827.2 % for gas demand and 102.4 % for electric peak power between design optimization and dynamic simulation are shown.

Keywords:

Energy hub; Linear programming design optimization; Dynamic simulation; Techno-economic analysis

1. Introduction

In Germany, district heating networks (DHN) are put into focus by policymakers and are a key element in German decarbonization strategy [1]. DHNs enable large potential in the reduction of greenhouse gas emissions [2]. In addition, retrofitting, e.g. improved building insulation, reduces space heating demand and contributes to potential supply temperature decrease [3]. According to Directive (EU) 2023/1791, buildings are to be insulated in the future in order to reduce CO_2 emissions. Fourth Generation DHN operate at low supply temperature levels, enabling the integration of various renewable heat sources and generation technologies [4], [5]. Future energy hub (EH) design must respect these aspects to increase the share of district heating.

The design and operation of EHs with multiple heat generation and storage technologies are complex, as economic and environmental objectives, the interaction of different energy carriers, as well as time-dependent demand and market connections must be considered [6]. In addition, uncertainties such as future energy carrier prices and the development of heat demand can influence EH design [7]. Also, legal regulations address the operation of existing and new DHNs regarding the share of fossil-based heat production [1]. Design optimizations such as linear programming (LP) or mixed-integer linear programming (MILP) are suitable to take all of these complex constraints into account [6], [8]. They enable an integration of multiple technologies, energy carriers and sectors [9]. The literature focuses on economic design optimization [7]. The evaluation of optimization methods and their results are addressed in various ways in the literature, as discussed below.

Wirtz et al. [8] compare 24 different optimization problems (LPs and MILPs) with respect to variations in investment costs, the decision of multiple components of the same technology, minimum part-load, part-load efficiency, and start-up costs. Their analysis for an EH shows that uncertainties increase as the level of detail decreases in simplified modelling of technology operation. Simple models as they are used in LPs use constant efficiencies or fundamental equations for the efficiency of a technology. In MILPs, load-dependent efficiencies and minimum part load affect the optimal results but lead to longer computation times. However, their results indicate that the influence of these aspects on technology sizing is quite small.

Hoffmann et al. [10] compare different temporal aggregation strategies used to reduce the computational complexity of energy system optimization models by representing time series using typical time steps, typical days, and typical weeks derived from clustering. The results show that although typical time steps perform better in terms of clustering indicators, the appropriate typical period depends on how storages are considered.

Thiran et al. [11] investigate the impact of typical day clustering on the results of energy system design optimization in a multi-regional energy system model. By comparing scenarios with different numbers of typical days, the authors show that using 10 typical days can reduce computational time up to 23.8 times faster while keeping the design error below 17 %. The results further indicate that the time-series error is a good predictor of the optimization results accuracy compared to results obtained using full-year data.

Next to design optimization, dynamic simulations are a valuable to for system analysis as they represent thermal inertias. This is particularly important for DHN and TES, which exhibit large thermal inertias. In addition, dynamic simulations can represent realistic control strategies. In contrast, design optimization is mainly based on energy and power balances [10]. Consequently, dynamic simulations enable a more realistic operation [12].

This work focuses on the difference in system operation modelling between design optimization and dynamic simulation, and how the differences in operation modelling affect decision indicators for techno-economic analysis. The analysis investigates centralized air-source heat pumps (ASHP) in combination with common heat generation technologies and their corresponding temperature levels in accordance with third generation DHN and fourth generation DHN.

2. Methodology

Figure 1 presents the overall methodology, which is divided into pre-simulation, EH design optimization (Opti_{12}), operational optimization (Opti_{365}), and dynamic simulation (Sim). The building individual dynamic pre-simulation of substations (SuSt) presents SuSt operation resulting in DHN thermal load $\dot{Q}^{\mathrm{DHN}}$ and additional heat generation $\dot{Q}^{\mathrm{SuSt}}$ for domestic hot water (DHW) provided by SuSt electricity P^{SuSt}. Consequently, both must match heat demand (dem) $\dot{Q}^{\mathrm{dem}}$. The $\dot{Q}^{\mathrm{dem}}$ consists of space heating (SH) and DHW. SH- and DHW time-series data are generated with an hourly resolution for a full year using *Districtgenerator* as presented by Henn et al [12].

$$\dot{Q}_{d,h}^{\mathrm{DHN}} + \dot{Q}_{d,h}^{\mathrm{SuSt}} = \dot{Q}_{d,h}^{\mathrm{dem}} = \dot{Q}_{d,h}^{\mathrm{dem,SH}} + \dot{Q}_{d,h}^{\mathrm{dem,DHW}} \quad \forall\, d \in \{1,\dots,365\}, h \in \{1,\dots,24\} \tag{1}$$

Consequently, for design optimization, the EH must supply $\dot{Q}^{\mathrm{DHN}}$ and, if required, the corresponding SuSt electricity supporting decentralized DHW supply. Opti_{12} is an LP that optimizes EH design by minimizing net present value PV. Opti_{12} uses a set of typical days $D = \{1,\dots,12\}$.

To evaluate full year operation, two approaches are introduced. A centralized ASHP is the main heat supplier in each configuration. The operational optimization Opti_{365} builds on the results and the LP model of Opti_{12} to determine optimal system operation over a full year $D = \{1,\dots,365\}$. In contrast to Opti_{12}, Opti_{365} maximizes thermal energy provided by the ASHP. Additionally, Sim performs a rule-based control in Modelica, prioritizing ASHP operation as well. Like Opti_{365}, the dynamic simulation uses the results of Opti_{12} for parameterization.

The LP formulation for Opti_{12} and Opti_{365} is described in Subsection 2.1, while the dynamic simulation approach is presented in Subsection 2.2.

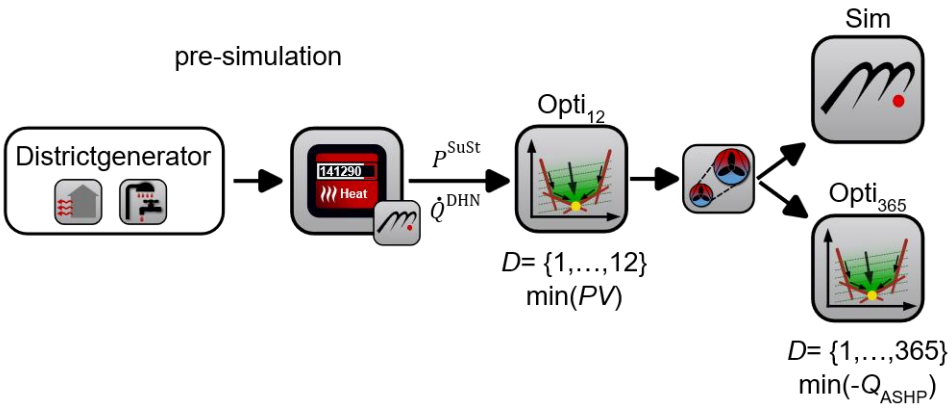

Figure 1: Overall methodology uses hourly time-series data to perform dynamic pre-simulations in SuSt, generating load profiles for DHN. Opti$_{12}$ is used to determine the optimal EH design from an economic perspective. The annual optimal operation is compared with the annual dynamic simulation, with both approaches prioritizing ASHP heat supply.

2.1 Linear Programming Model

The literature presents numerous LP models. This work bases on the LP model EHDO, presented by Wirtz et al. [13]. This subsection describes the refactoring and adaptations implemented for this study. In particular, the EHDO model is simplified by focusing only on ASHP, Gas Boiler (GB), Electric Boiler (EB), Combined Heat and Power (CHP) units, and thermal energy storage (TES).

2.1.1 Objective function

The objective function aims to minimize the net PV of the investment I. All technologies in the EH are denoted by $t \in \mathrm{T}$, while the project years are represented by $\mathrm{y} \in \mathrm{Y}$. Since values for I are incurred at the beginning of the project period, discounting is applied only to the operational expenditure C^{OPEX} assuming a constant discounting rate r.

$$\min PV = \sum_{t \in T} \left(I_t + \sum_{y \in Y} \frac{C_{y,t}^{\mathrm{OPEX}}}{(1+r)^y} \right) \tag{2}$$

In contrast, Opti$_{365}$ uses the following objective function to maximize ASHP heat generation.

$$\min(-Q_{ASHP}) \tag{3}$$

2.1.2 Costs

Investment costs strongly depend on the nominal capacity of the installed technologies [14]. However, LP models require specific investment costs to be independent of the resulting capacities [8]. Since most investment cost functions are non-linear [14], an MILP formulation could linearize them in a piecewise manner [8]. However, this introduces additional modeling effort and approximation errors due to the linearization, while also increasing computational time [8]. To simplify the formulation while still accounting for capacity-dependent specific investment costs while maintaining the computational advantages of LP compared to MILP, an iterative approach is applied. In each iteration n, the specific investment costs i are passed to the LP and subsequently adjusted based on the resulting nominal capacities. Convergence between input and output values is achieved when the deviation falls below a predefined threshold of 5 % for all technologies.

$$\max_{t \in T} \frac{\left| i_{n,t} - i_{(n-1),t} \right|}{\frac{i_{n,t} + i_{(n-1),t}}{2}} \leq 5\ \% \tag{4}$$

The operational expenditure OPEX consists of the energy carrier costs C^{ec} and fixed maintenance costs C^{fix}.

$$C^{\mathrm{OPEX}} = C^{\mathrm{ec}} + C^{\mathrm{fix}} \tag{5}$$

Four different energy carriers are investigated: electricity import from the grid, electricity export to the grid, natural gas (NG) and biogas (BG). For simplifications, all prices are assumed to remain constant over project duration, resulting in equal annual C^{ec}.

$$C^{\mathrm{ec}} = C^{\mathrm{NG}} + C^{\mathrm{BG}} + C^{\mathrm{import}} - C^{\mathrm{export}} \tag{6}$$

2.1.3 Heat generation technologies

Different heat generation technologies are taken into account. For the ASHP, the Coefficient of Performance (COP) is taken from characteristic chart, that is also used in dynamic simulation. The characteristic chart is based on a simplified model of a simple refrigerant cycle. For design optimization, the COP can be taken as a function of supply and source temperatures based on this chart. Compressor part-load dependencies are not considered by the characteristic chart.

$$\dot{Q}_{d,h}^{\mathrm{ASHP}} = COP_{d,h}^{\mathrm{ASHP}} \cdot P_{d,h}^{\mathrm{ASHP}} \; \forall \, h \in \{1, \dots, 24\}, d \in D \tag{7}$$

The CHP efficiencies chart is modelled in a simplified way, considering electric efficiency $\eta_{\mathrm{el}}^{\mathrm{CHP}}$ and thermal efficiency $\eta_{\mathrm{th}}^{\mathrm{CHP}}$ as a function of the nominal electric capacity. Part-load dependencies are neglected in optimization. Since the LP model is iteratively initialized (Equation 4), new nominal CHP efficiencies can be passed to the LP at the beginning of each iteration.

$$P_{d,\mathrm{h}}^{\mathrm{CHP}} = \eta_{\mathrm{el}}^{\mathrm{CHP}} \cdot (F_{d,h}^{\mathrm{CHP,NG}} + F_{d,h}^{\mathrm{CHP,BG}}) = \eta_{\mathrm{el}}^{\mathrm{CHP}} \cdot \frac{\dot{Q}_{d,\mathrm{h}}^{\mathrm{CHP}}}{\eta_{\mathrm{th}}^{\mathrm{CHP}}} \; \forall \, h \in \{1, \dots, 24\}, d \in D \tag{8}$$

The GB model uses a capacity independent thermal efficiency.

$$\dot{Q}_{d,\mathrm{h}}^{\mathrm{GB}} = \eta_{\mathrm{th}}^{\mathrm{GB}} \cdot F_{d,h}^{\mathrm{GB}} \; \forall \, h \in \{1, \dots, 24\}, d \in D \tag{9}$$

2.1.4 Energy balances

This subsection presents all relevant energy balances. The sum of all heat producers, TES charging, and discharging must match with the heat supply of the DHN at each time step.

$$\dot{Q}_{d,h}^{\mathrm{DHN}} + Q_{d,h}^{\mathrm{TES,charge}} = \dot{Q}_{d,h}^{\mathrm{CHP}} + \dot{Q}_{d,h}^{\mathrm{ASHP}} + \dot{Q}_{d,h}^{\mathrm{EB}} + \dot{Q}_{d,h}^{\mathrm{GB}} + \dot{Q}_{d,h}^{\mathrm{TES,discharge}} \forall \, h \in \{1, \dots, 24\}, d \in D \tag{10}$$

The LP is extended to include $P_{d,\mathrm{h}}^{\mathrm{SuSt}}$, as electricity must be supplied by the DHN operator, resulting in an increased share of total electricity demand.

$$P_{d,h}^{\mathrm{import}} + P_{d,h}^{\mathrm{CHP}} = P_{d,h}^{\mathrm{SuSt}} + P_{d,h}^{\mathrm{ASHP}} + P_{d,h}^{\mathrm{EB}} + P_{d,h}^{\mathrm{export}} \; \forall \, h \in \{1, \dots, 24\}, d \in D \tag{11}$$

As the legal framework specifies allowed shares of NG and BG [1], the gas demand F is distinguished by fuel type, NG and BG.

$$F_{d,h}^{\mathrm{NG}} = \frac{\dot{Q}_{d,h}^{\mathrm{CHP,NG}}}{\eta_{\mathrm{th}}^{\mathrm{CHP}}} + \frac{\dot{Q}_{d,h}^{\mathrm{GB,NG}}}{\eta_{\mathrm{th}}^{\mathrm{GB}}} \; \forall \, h \in \{1, \dots, 24\}, d \in D \tag{12}$$

$$F_{d,h}^{\mathrm{BG}} = \frac{\dot{Q}_{d,h}^{\mathrm{CHP,BG}}}{\eta_{\mathrm{th}}^{\mathrm{CHP}}} + \frac{\dot{Q}_{d,h}^{\mathrm{GB,BG}}}{\eta_{\mathrm{th}}^{\mathrm{GB}}} \; \forall \, h \in \{1, \dots, 24\}, d \in D \tag{13}$$

2.1.5 Constraints

The nominal power of all heat generators must be equal to the maximum of the DHN thermal load and the nominal heat load of all buildings. This nominal heat load is based on DIN EN 12831-1:201709 [12].

$$max\left(\dot{Q}_{\mathrm{nom}}^{\mathrm{dem,SH}}, \dot{Q}_{\mathrm{max}}^{\mathrm{DHN}}\right) = \dot{Q}_{\mathrm{nom}}^{\mathrm{CHP}} + \dot{Q}_{\mathrm{nom}}^{\mathrm{ASHP}} + \dot{Q}_{\mathrm{nom}}^{\mathrm{GB}} + \dot{Q}_{\mathrm{nom}}^{\mathrm{EB}} \tag{14}$$

The TES capacity E^{TES} is limited to a minimum specific volume of $0.025 \frac{\mathrm{m^3}}{\mathrm{kW_{nom}}}$ [15] for a constant temperature difference ΔT^{nom}=5 K. This corresponds to the assumed temperature difference in the ASHP condenser.

$$E^{\mathrm{TES}} \geq 0.025 \frac{\mathrm{m^3}}{\mathrm{kW_{nom}}} \cdot max\left(\dot{Q}_{\mathrm{nom}}^{\mathrm{dem,SH}}, \dot{Q}_{\mathrm{max}}^{\mathrm{DHN}}\right) \cdot c_p \cdot \rho \cdot \Delta T^{\mathrm{nom}} \tag{15}$$

As introduced, German law regulates the composition of heat in a DHN through two legal frameworks [1]: the renewable share of Q^{DHN} must exceed 65 %, and the share of biomass-based heat in Q^{DHN} must not exceed 25 % for a total DHN length greater than 50 km. Both constraints are only active for Opti_{12}.

$$Q^{\mathrm{DHN}} \cdot 65\,\% \leq Q^{\mathrm{ASHP}} + Q^{\mathrm{EB}} + Q^{\mathrm{GB,BG}} + Q^{\mathrm{CHP,BG}} \tag{16}$$

$$Q^{\mathrm{DHN}} \cdot 25\,\% \geq Q^{\mathrm{GB,BG}} + Q^{\mathrm{CHP,BG}} \tag{17}$$

In addition, to avoid high electricity peaks, a maximum share of 10 % is assumed for EB.

$$Q^{\mathrm{DHN}} \cdot 10\,\% \geq Q^{\mathrm{EB}} \tag{18}$$

2.2 Dynamic Simulation

A modular EH model in combination with a simplified DHN model is used for dynamic simulation in Modelica. The EH model consists of four modular heat generation models: ASHP, GB, CHP, and EB. A corresponding characteristic chart is implemented to describe detailed ASHP operation as mentioned in Subsection 2.1.3. To match parameterization with Opti_{12} results, the EH model enables simple and user-friendly parameterization, as described by Zuschlag et al. [16], based solely on nominal operating conditions.

In contrast to Opti_{365} objective function (Equation 3), this paragraph introduces rule-based control strategy of dynamic simulation. In the EH model, the heat generation technologies ASHP, GB, and CHP are connected parallelly, loading the TES directly with no heat exchanger. In contrast, the EB operates between the outlet of the TES top layer and the DHN model. A modular TES control strategy prioritizes ASHP heat supply. This control is divided into base-load mode and peak-load mode. Figure 2 describes base-load and peak-load. If ASHP power is sufficient to meet heat demand, the TES can be divided into two layers: a hot buffer layer and a cold layer. If the heat demand exceeds the full load thermal power of the ASHP, cold layer increases. A temperature sensor detects the resulting buffer layer decrease and initiates peak-load operation. During peak-load, additional heat generation is activated, either CHP or GB. Peak-load performs as long as the lowest temperature sensor detects $T_{\mathrm{set}}^{\mathrm{DHN}}$.

For control simplification, the EB is not integrated into TES control strategy as EB operates between TES and DHN. Consequently, if the temperature of the top layer does not match $T_{\mathrm{set}}^{\mathrm{DHN}}$, the EB automatically provides missing temperature difference $T_{\mathrm{set}}^{\mathrm{DHN}} - T_{\mathrm{top\,layer}}^{\mathrm{TES}}$.

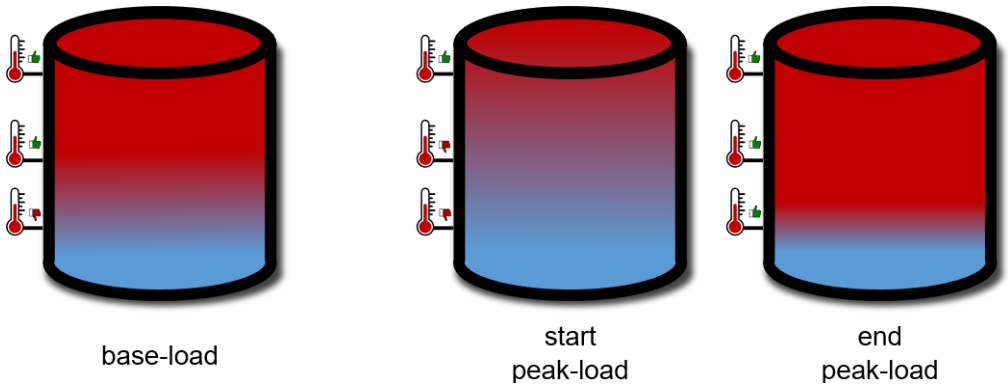

Figure 2: Rule-based TES control strategy in the dynamic Simulation for base-load and peak-load operation

The DHN is modeled in a simplified manner using two volumes representing the supply and return networks.

2.3 Comparison Indicators

The optimization and simulation results are evaluated using techno-economic analysis. From a technical perspective, energy carrier demand and electric peak load are assessed to characterize system operation. To place the operation in an economic context, the levelized cost of heat (LCOH) is used, capturing both operational and capital expenditures [17].

$$LCOH = \frac{PV}{\sum_{y \in Y} \frac{Q_y^{\mathrm{dem}}}{(1+r)^y}} \tag{19}$$

2.4 Use case

A residential neighborhood based on Integranet type 1 is used [18]. Table 1 presents the respective nominal parameters. The nominal heat load is derived from building-specific heat load calculations performed with the *Districtgenerator* tool [12]. Three building states are investigated: Construction, Retrofit and Retrofit+. Only nominal temperatures of the construction state are assumed for decentralized condition 70/55 °C. In contrast, the nominal supply and return temperature for both retrofit cases are determined based on the corresponding reduction in nominal heat load, as presented by Lämmle et al. [3]. In addition, nominal temperatures account for additional heat losses as well as a temperature difference required for heat transfer resulting in presented values. The nominal temperatures belong either to third generation DHN or fourth generation DHN.

Table 1: Nominal district parameters for construction states: Construction / Retrofit / Retrofit+

$\dot{Q}_{\mathrm{nom}}^{\mathrm{dem}}$ in kW	$T_{\mathrm{nom}}^{\mathrm{supply}}$ in °C	$T_{\mathrm{nom}}^{\mathrm{return}}$ in °C
1,796 / 705 / 541	75.62 / 54.12 / 49.78	59.53 / 47.24 / 44.25

For the EH, multiple predefined sets of heat generation technologies are considered, for which Opti_{12} determines the optimal system sizes. Table 2 presents all parameter values as calculated by Opti_{12}, which serve as constraints for Opti_{365} (apart from $T_{\mathrm{nom}}^{\mathrm{source}}$) and as parameter values for the EH model for dynamic simulation. In total, 12 different EH configurations are investigated.

Table 2: Parameters of the technologies for construction states: Construction / Retrofit / Retrofit+

Parameter		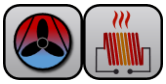		
V^{TES} in m³	44.91 / 17.63 / 15.66	44.91 / 17.63 / 24.67	44.91 / 17.63 / 15.66	44.91 / 17.63 / 15.66
$\dot{Q}_{\mathrm{nom}}^{\mathrm{ASHP}}$ in kW	1,796 / 705 / 626	1,022 / 364 / 267	982 / 335 / 258	1,371 / 455 / 284
$T_{\mathrm{nom}}^{\mathrm{source}}$ in °C	5.6 / 5.6 / −1.2	−4.4 / −4.4 / −5.7	−5.1 / −5.7 / −5.7	3.5 / −1.1 / −4.4
$\dot{Q}_{\mathrm{nom}}^{\mathrm{EB}}$ in kW		774 / 341 / 360		
$\dot{Q}_{\mathrm{nom}}^{\mathrm{GB}}$ in kW			815 / 370 / 369	
$P_{\mathrm{nom}}^{\mathrm{CHP}}$ in KW				288 / 162 / 230

3. Results

In this section, first Subsection 3.1 evaluates the rule-based control strategy. Subsequently, Subsections 3.2 and 3.3 present the techno-economic analysis of multiple performance indicators, comparing the results of Opti_{12}, Opti_{365}, and Sim.

3.1 Analysis of rule-based control

Figure 3 illustrates the annual DHN supply temperature profiles. The controlled variable for the heat generation technologies ASHP & CHP is presented as representative example. Retrofitting leads to a reduction in supply temperature.

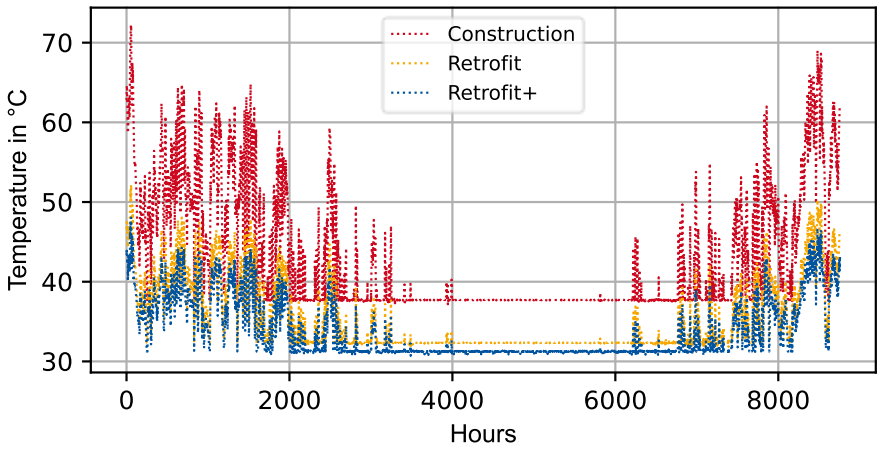

Figure 3: Annual DHN supply temperature (controlled variable), illustrated for EH combination ASHP & CHP

Table 3 presents, for all construction states and all EH configurations, the root mean square error (RMSE) between the DHN supply temperature and the corresponding setpoint. In addition, the maximum positive and negative deviations, and $T_{\mathrm{nom}}^{\mathrm{source}}$ values as calculated by Opti_{12} (see Table 2) and Opti_{365} are shown.

The negative deviation of −20.97 K in the case ASHP only & Retrofit results from an excessively high $T_{\mathrm{nom}}^{\mathrm{source}}$=5.6 °C compared to $T_{\mathrm{nom}}^{\mathrm{source}}$=−0.8 °C for Opti_{365}. As this indicates, the operational mapping of Opti_{12} shifts the maximum ASHP thermal power toward warmer $T_{\mathrm{nom}}^{\mathrm{source}}$, mainly for the ASHP only mapping. Since the maximum ASHP thermal power depends on operating conditions, ASHP is insufficient in the dynamic simulation on certain cold days. This leads to a mismatch in $\dot{Q}^{\mathrm{DHN}}$ despite the presence of TES. In contrast, for Construction, the TES is sufficient to compensate for the mismatch between the ASHP and $\dot{Q}^{\mathrm{DHN}}$ on cold days, as the negative deviation is only −0.76 K. Even though $T_{\mathrm{nom}}^{\mathrm{source}}$=3.5 °C is specified for the ASHP & CHP Construction case, the CHP can compensate for reduced ASHP operation, as the negative deviation is only −0.77 K. These cases highlight the capability of dynamic simulation for validation purposes, if it respects a more complex ASHP operation characteristic than LP optimization.

The positive deviations, in turn, are caused by inertia and DHN control, as the supply temperature does not cool down quickly enough despite return flow mixing. Since all RMSE values are below 1 K, events with negative or positive deviations cover only small time periods compared to full year simulation.

Table 3: RMSE for the EH configurations and construction states: Construction / Retrofit / Retrofit+

Indicator				
RMSE in K	0.08 / 0.78 / 0.15	0.07 / 0.04 / 0.04	0.15 / 0.16 / 0.20	0.08 / 0.07 / 0.18
Pos. deviation in K	2.48 / 1.35 / 1.12	2.53 / 1.42 / 1.31	2.54 / 1.44 / 1.26	2.50 / 1.40 / 1.23
Neg. deviation. in K	−0.76 / −20.97 / −0.66	−0.84 / -0.67 / −0.57	−2.93 / −2.12 / −2.21	−0.77 / −0.95 / −2.02
Opti_{12} $T_{\mathrm{nom}}^{\mathrm{source}}$ in °C	5.6 / 5.6 / −1.2	−4.4 / −4.4 / −5.7	−5.1 / −5.7 / −5.7	3.5 / −1.1 / −4.4
Opti_{365} $T_{\mathrm{nom}}^{\mathrm{source}}$ in °C	−5.7 / −0.8 / −0.8	-5.7 / -5.7 / −5.7	−5.7 / −5.7 / −5.7	−5.7 / −5.7 / −5.7

3.2 Technical analysis

The analysis regarding technical aspects covers electricity and gas demand. Figure 4 presents annual electric energy demand for all considered combinations of heat generation technologies and building states. Subfigure (a) shows monovalent ASHP, Subfigure (b) ASHP & EB, Subfigure (c) ASHP & GB, and Subfigure (d) ASHP & CHP. On the x-axis, $Opti_{12}$, $Opti_{365}$, and Sim correspond to the respective building states. Since $Opti_{12}$ sets parameters for $Opti_{365}$ and Sim, on top of each bar the percentage difference referring to $Opti_{12}$ is added. Overall, annual electric energy demand differs between −20.3 % and −5.1 % in reference to $Opti_{12}$.

Notably, $Opti_{365}$ and Sim are mostly in closer agreement with each other than either is with $Opti_{12}$. In contrast, the results from $Opti_{365}$ are consistently lower than those of Sim except for ASHP & EB. In conclusion, for most cases representing 365 days in $Opti_{365}$ lead to a higher agreement with the results of the annual dynamic simulation.

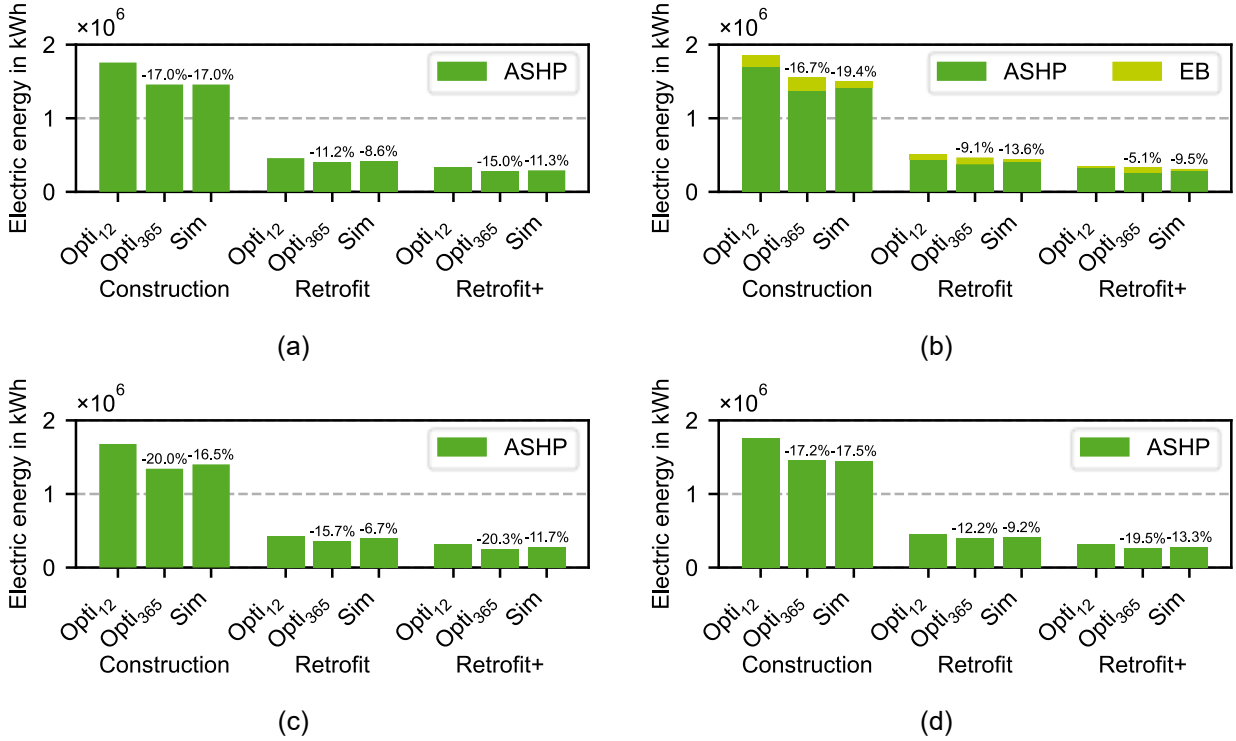

Figure 4: Annual electric energy demand: ASHP (a), ASHP & EB (b), ASHP & GB (c), and ASHP & CHP (d)

In addition to annual electric energy demand, Figure 5 illustrates electric peak power. Overall, the electric peak power deviates between 102.4 % and −17.9 % compared to $Opti_{12}$. The largest deviations occur for ASHP only (Subfigure (a)) and the ASHP & EB combination (Subfigure (b)). Consequently, the only electricity heat supply combinations result in high deviations. In addition, most of the results of $Opti_{365}$ and Sim are closer to each other. Additionally, Subfigure (a) highlights the mismatch of ASHP thermal power and DHN heat demand, as initially discussed for Table 3. In comparison to Subfigures (b), peak electric power deviates significantly, due to the higher $T_{\text{nom}}^{\text{source}}$. Subfigure (b), in contrast, shows good agreement in ASHP peak power values but a mismatch in EB peak power values. A different picture emerges for the hybrid system configurations in Subfigures (c) and (d). Addressing $T_{\text{nom}}^{\text{source}}$ and ASHP peak power, a similar effect is also observed in Subfigure (d).

Overall, it can be concluded that representing the full year instead of 12 typical days leads to an improved agreement in general, as ASHP operating is better captured. However, thermal inertias and peak load operation can still cause discrepancies between $Opti_{365}$ and Sim.

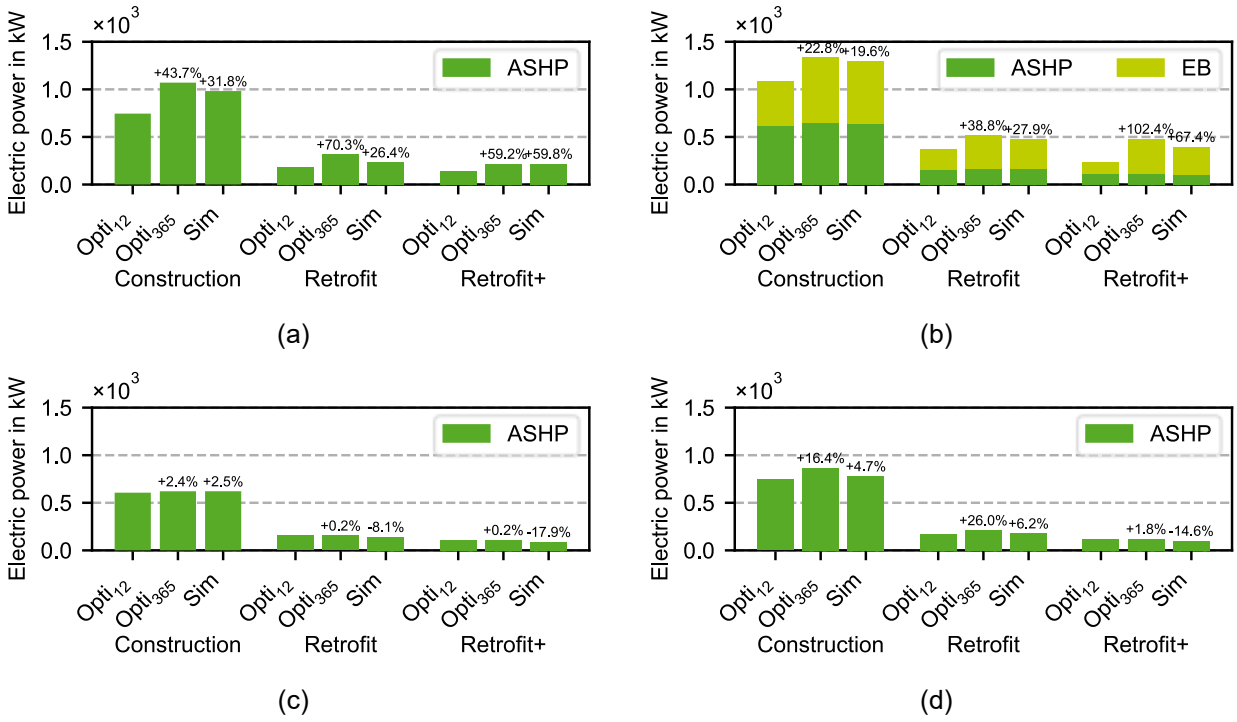

Figure 5: Peak electric power: ASHP (a), ASHP & EB (b), ASHP & GB (c), and ASHP & CHP (d)

The annual gas demand is presented by Figure 6. In comparison to previous indicators, results deviate highly up to 3827.2 %. Except for the construction state for ASHP & CHP, the optimal operation in Opti$_{365}$ consistently shows larger gas demand values than Sim. Since both Opti$_{365}$ and Sim prioritize the use of the ASHP, the observed differences can be attributed to the discrepancy between quasi-steady-state modeling and dynamic system representation, as well as to differences in the state of charge of the TES. Except for the construction state for ASHP & CHP, system inertia like DHN and TES allows for less operation of peak load heat generation units in Sim. This effect is also evident in Figure 4 (b), where the electric energy demand of both ASHP and EB, are consistently lower in Sim results than in Opti$_{365}$ results. Similarly, the peak electric power is reduced in Sim compared to Opti$_{365}$, as shown in Figure 5 (b). Additionally, Figure 4 (c) indicates more ASHP operation for Sim than for Opti$_{365}$.

In contrast, the TES control strategy results in more CHP operation for ASHP & CHP construction state than with Opti$_{365}$. This agrees with less ASHP operation in Sim than in Opti$_{365}$ as presented by Figure 4 (d). In addition to the TES control strategy, $T_{\text{nom}}^{\text{source}}$ is relatively high, resulting in smaller thermal ASHP power on cold days in Sim compared to the Opti$_{12}$ predictions.

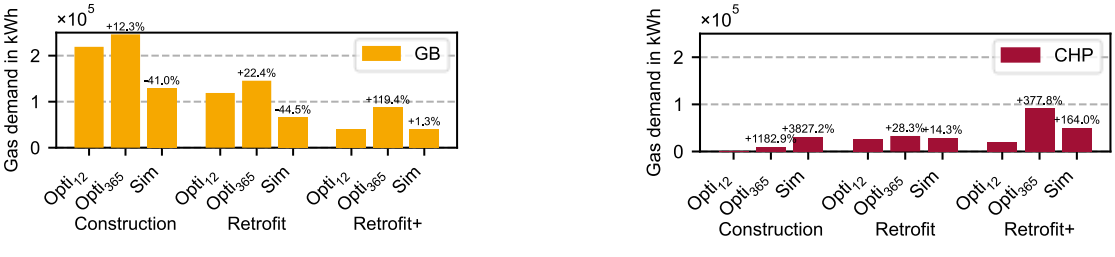

Figure 6: Annual gas demand: ASHP & GB (a) and ASHP & CHP (b)

3.3 Economic analysis

Figure 7 illustrates LCOH for all cases. LCOH is composed of capital costs and operational costs. All LCOH values are calculated based on interpolated and therefore continuous heat demands derived from load profiles of SuSt pre-simulation. This facilitates a consistent comparison of operational results. The overall relative deviations of Opti$_{365}$ and Sim from Opti$_{12}$ ranges between −12.5 % and −2.3 %. Specific investment costs are consistently equal between the three methods as they are based on Opti$_{12}$ results. It should be noted that

$Opti_{12}$ generally overestimates LCOH, while the results of $Opti_{365}$ and Sim are mostly closer to each other. In combination with analyzed annual energy demands, this indicates that the applied number of typical days has a greater impact on economic assessment than the dynamic representation.

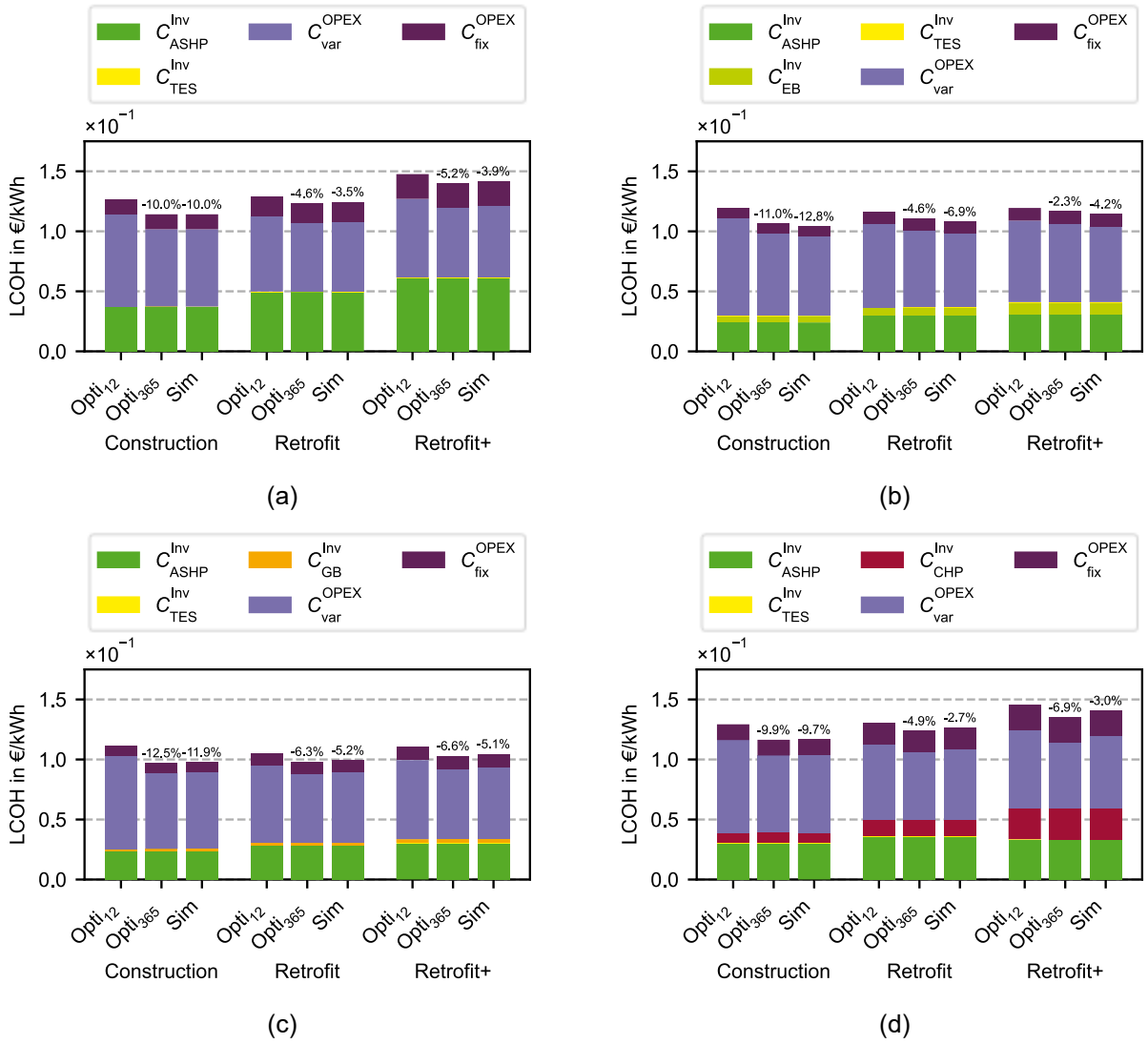

Figure 7: Composition of LCOH: ASHP (a), ASHP & EB (b), ASHP & GB (c), and ASHP & CHP (d)

4. Discussion

The comparison of design optimization, optimal operation, and dynamic simulation is subject to several sources of uncertainty. Although the ASHP models are based on identical COP data, the optimizations do not fully capture the physical limitations of the heat pump. This influences full-load operation description at source temperatures higher than nominal conditions, as optimization underestimates thermal power in comparison to dynamic simulation. Furthermore, the optimal operation does not account for minimum part-load constraints. While ASHP and GB can be assumed to operate in multiple units, this limitation primarily affects CHP, as its minimum electrical part-load in dynamic simulation is 50 %. Additionally, part-load behavior and temperature-dependent efficiency effects are only captured in the dynamic simulation model. To achieve good agreement between methods, it is essential that the efficiency models of each heat generation technology are consistent across optimization and simulation.

The analysis does not account for differences in time-series data integration. The dynamic simulation uses linear interpolation between time steps, whereas the optimization considers stepwise values. Consequently, the two methods yield different annual heat demand results.

Since the system design is constrained by the maximum thermal capacity of DHN and the nominal heat demand of all connected buildings, the EH thermal capacity is consistently sufficient. As a result, the system—particularly in configurations relying solely on ASHP or in combination with CHP—tends to be oversized,

provided that the nominal supply and heat source temperatures are adequately accounted for. The EH design and operation prioritize ASHP. In a more balanced system, differences in secondary heat supply could have a greater impact. In addition, this effect is influenced by the TES capacity, which variation is not examined in detail in this study.

Constant energy carrier prices are assumed for comparison purposes, which corresponds well with the application of rule-based control strategies. Dynamic pricing could significantly influence the results for both unchanged control approach and more sophisticated approaches exploiting pricing information. Since $Opti_{12}$ optimizes economic operation, the comparison between $Opti_{12}$ and $Opti_{365}$ is highly influenced by the objective function resulting in different operational behavior which was not discussed in detail.

5. Conclusion

In this work, three different approaches for predicting system operation are analyzed across 12 energy hub configurations. The LP design optimization $Opti_{12}$ uses 12 typical days. Building on this, the optimal quasi-static operation of $Opti_{365}$ covers an entire year. Simultaneously, the dynamic simulation Sim uses the selected system design. The indicators electric energy demand, peak electric power, gas demand, and LCOH are discussed.

The analysis of technical and economic indicators shows that the three approaches lead to large deviations in operational indicators, while deviations in LCOH are smaller. The DHN temperatures are adequately supplied by the EH, indicating that the systems are not undersized by $Opti_{12}$. Only design operating conditions for ASHP have a large impact, that can result in mismatch of ASHP thermal power and DHN demand in the dynamic simulation on cold days. Additional operational differences address mainly the peak load heat technologies EB, GB and CHP. In particular, the differences for GB and CHP are significant, as their utilization is strongly influenced by the TES control strategy, thermal inertias and clustering. The gas demand of the CHP unit shows the largest deviation, with $Opti_{12}$ significantly underestimating CHP gas consumption. However, the impact on LCOH remains limited and is primarily attributable to the clustering approach, as $Opti_{365}$ and the dynamic simulation show strong agreement. Overall, clustering leads to a slight overestimation of LCOH compared to both $Opti_{365}$ and Sim.

In summary, this work demonstrates that dynamic simulations—particularly for representing operational behavior—can effectively support and validate the conclusions of design optimization and belonging operational optimization. Representing an additional full year of operation improves the accuracy of the design optimization results compared to simulation results in hourly resolution, particularly with respect to peak loads. For a peak load operator, a dynamic simulation emphasizes operation for both power and energy demand, especially for additional gas based, hydraulically integrated technologies. Due to thermal inertia, rule-based dynamic control can achieve lower energy and peak-power demand than optimization-based approaches that assume quasi-static operation under peak-load conditions. Future work can address TES capacity variations, TES charging and discharging, and analyzing differences in temporal aggregations methods for typical days.

Nomenclature

Acronyms		**Subscripts and Superscripts**	
DHN	district heating networks	el	electrical
LP	linear programming	th	thermal
MILP	mixed-integer linear programming	Inv	Investment
Sim	simulation	OPEX	Operational expenditure
Opti	optimization	nom	nominal
ASHP &	air source heat pump	ec	energy carrier
GB	gas boiler	NG	natural gas
EH	energy hub	BG	biogas
CHP	combined heat and power	var	variable
EB	electric boiler	dem	demand
LCOH	levelized cost of heat		
SuSt	substation		
TES	thermal energy storage		
SH	space heating		
DHW	domestic hot water		
RMSE	root mean square error		

Symbols			
COP	coefficient of performance, -	I	investment, €
C	cost, €	c_p	specific heat capacity, kj kg^{-1} K^{-1}
PV	present value, €	ρ	density, kg m^{-3}
T	temperature, °C	ΔT	temperature difference, K
Q	thermal energy, kWh	η	efficiency
$\dot{Q}$	thermal power, kW	**Indices and sets**	
P	electric power, kW	n	iteration count
F	gas energy, kWh	h	hour
r	discount rate, %	$d \in D$	day
E	Thermal capacity, kWh	$y \in Y$	year
i	specific investment cost, € kW^{-1} or € m^{-3}	$t \in T$	technology
V	volume, m³		

Acknowledgement

We gratefully acknowledge the financial support by the German Federal Ministry for Economic Affairs and Energy (BMWE), promotional reference 03EN3080C.

References

[1] *Wärmeplanungsgesetz vom 20. Dezember 2023 (BGBl. 2023 I Nr. 394)*. 01.01.2024.

[2] U. Persson, E. Wiechers, B. Möller, und S. Werner, „Heat Roadmap Europe: Heat distribution costs“, *Energy*, Bd. 176, S. 604–622, Juni 2019, doi: 10.1016/j.energy.2019.03.189.

[3] M. Lämmle *u. a.*, „Performance of air and ground source heat pumps retrofitted to radiator heating systems and measures to reduce space heating temperatures in existing buildings“, *Energy*, Bd. 242, S. 122952, März 2022, doi: 10.1016/j.energy.2021.122952.

[4] M. Wirtz, L. Kivilip, P. Remmen, und D. Müller, „Quantifying Demand Balancing in Bidirectional Low Temperature Networks“, *Energy and Buildings*, Bd. 224, S. 110245, Okt. 2020, doi: 10.1016/j.enbuild.2020.110245.

[5] H. Lund *u. a.*, „4th Generation District Heating (4GDH) Integrating smart thermal grids into future sustainable energy systems“, *Energy*, Bd. 68, S. 1–11, Apr. 2014, doi: 10.1016/j.energy.2014.02.089.

[6] C. Papadimitriou *u. a.*, „A Comprehensive Review of the Design and Operation Optimization of Energy Hubs and Their Interaction with the Markets and External Networks“, *Energies*, Bd. 16, Nr. 10, S. 4018, Mai 2023, doi: 10.3390/en16104018.

[7] M. Kiani-Moghaddam, M. N. Soltani, S. A. Kalogirou, und A. Arabkoohsar, „A review of optimization efforts on neighborhood-level energy hubs“, *Energy*, Bd. 317, S. 134657, Feb. 2025, doi: 10.1016/j.energy.2025.134657.

[8] M. Wirtz, M. Hahn, T. Schreiber, und D. Müller, „Design optimization of multi-energy systems using mixed-integer linear programming: Which model complexity and level of detail is sufficient?“, *Energy Conversion and Management*, Bd. 240, S. 114249, Juli 2021, doi: 10.1016/j.enconman.2021.114249.

[9] A. Maroufmashat, S. Taqvi, A. Miragha, M. Fowler, und A. Elkamel, „Modeling and Optimization of Energy Hubs: A Comprehensive Review“, *Inventions*, Bd. 4, Nr. 3, S. 50, Aug. 2019, doi: 10.3390/inventions4030050.

[10] M. Geidl und G. Andersson, „Optimal Coupling of Energy Infrastructures“, in *2007 IEEE Lausanne Power Tech*, Lausanne, Switzerland: IEEE, Juli 2007, S. 1398–1403. doi: 10.1109/PCT.2007.4538520.

[11] J. Vieth, J. Westphal, und A. Speerforck, „District heating network topology optimization and optimal co-planning using dynamic simulations“, *Advances in Applied Energy*, Bd. 19, S. 100233, Sep. 2025, doi: 10.1016/j.adapen.2025.100233.

[12] S. Henn, J. D. Schölzel, T. Beckhölter, C. Wüller, R. Hamze, und D. Müller, „Districtgenerator: Generating building-specific load profiles for residential districts.“, *JOSS*, Bd. 10, Nr. 111, S. 7657, Juli 2025, doi: 10.21105/joss.07657.

[13] M. Wirtz, P. Remmen, und D. Müller, „EHDO: A free and open-source webtool for designing and optimizing multi-energy systems based on MILP“, *Comput Appl Eng Educ*, Bd. 29, Nr. 5, S. 983–993, Sep. 2021, doi: 10.1002/cae.22352.

[14] N. Langreder, F. Lettow, M. Sahnoun, S. Kreidelmeyer, A. Wünsch, und S. Lengning, „Technikkatalog Wärmeplanung 1.1“. ifeu – Institut für Energie- und Umweltforschung Heidelberg, Öko-Institut e.V., IER Stuttgart, adelphi consult GmbH, Becker Büttner Held PartGmbB, Prognos AG, 2024.

[15] F. Wüllhorst, J. Reuter-Schniete, L. Maier, und D. Müller, „Heat pump and thermal energy storage: Influences of photovoltaic, the control strategy, and price assumptions on the optimal design“, *Renewable Energy*, Bd. 236, S. 121409, Dez. 2024, doi: 10.1016/j.renene.2024.121409.

[16] M. Zuschlag, D. Jansen, R. Streblow, und D. Müller, „A user-friendly boiler model for dynamic simulations“, *Journal of Building Performance Simulation*, S. 1–19, Okt. 2025, doi: 10.1080/19401493.2025.2572693.

[17] J. Aldersey-Williams und T. Rubert, „Levelised cost of energy – A theoretical justification and critical assessment“, *Energy Policy*, Bd. 124, S. 169–179, Jan. 2019, doi: 10.1016/j.enpol.2018.10.004.

[18] J. Benthin *u. a.*, „Integrierte Betrachtung von Strom-, Gas- und Wärmesystemen zur modellbasierten Optimierung des Energieausgleichs- und Transportbedarfs innerhalb der deutschen Energienetze“, Fraunhofer UMSICHT, Gemeinsamer Abschlussbericht, März 2020.